Signal-to-Noise Ratio of CABRI Hodoscope: Monte Carlo Calculation Versus Experiments

Jacques Di Salvo, Salvatore Mirotta, Vincent Chevalier

Signal-to-Noise Ratio of CABRI hodoscope: Monte Carlo calculation versus experiments

J. Di Salvo, S. Mirotta, and V. Chevalier

***Abstract*—The CABRI experimental pulse reactor is devoted to the study of Reactivity Initiated Accidents (RIA), for the purpose of the CABRI International Program (CIP), managed by the French Radioprotection and Nuclear Safety Institute (IRSN). CABRI's hodoscope equipment detects the fast neutrons emitted during a power pulse by a tested rod, positioned inside a dedicated test loop reproducing either sodium reactor or Pressurized Water Reactor (PWR) conditions. One of the most important parameter measured by the hodoscope detectors is the Signal-to-Noise Ratio (SNR), characterizing the fraction of neutrons directly coming from the test rod ("signal") over neutrons coming from the core ("noise").**

In this article, the method used to calculate the SNR using a 2D model of CABRI, with the MCNP6.2 Monte Carlo code, will be detailed. Comparisons between the calculated and measured SNR for different configurations are in quite good agreement.

Another parameter of interest is the so-called "scattering coefficient", which corresponds to the fraction of neutrons coming from the test rod and being scattered between their birth and their detection. This parameter is used to enhance the analysis of the fuel displacement that may happen during the power transient.

To estimate this coefficient, an innovative method using a combination of different options available in MCNP6.2 has been used. Computed coefficients shows a slight discrepancy with the measurements.

Finally, sensitivity of the SNR and scattering coefficient to technological parameters and nuclear data libraries is discussed.

***Index Terms*— CABRI, Hodoscope, RIA transient**

I. Introduction

FOR enhancing safety of Nuclear Power Plants (NPP), the French Nuclear Safety and Radiation Protection Institute (IRSN) carries out experimental programs in order to improve the understanding of the fuel behavior under accident conditions. One of them is the CABRI International Program, managed and funded by IRSN under the OECD/NEA umbrella. The program is devoted to the study of Reactivity Initiated Accidents (RIA) in representative Pressurized Water Reactor (PWR) conditions [1].

The CABRI pool type reactor, located at the Cadarache nuclear research center, southern France, is designed to submit to a RIA a test rod, placed into the center of the core. To be representative of PWR conditions, a huge renovation of the CABRI facility, has been conducted by the French Alternative and Atomic Energies (CEA), its operator. This operation consisted of replacing the previous sodium loop, used for many past programs of the CABRI reactor, by a new one reproducing the thermal and hydraulic conditions met inside a PWR.

The power transients are generated by the unique reactivity injection system of CABRI [2]. 96 tubes (so-called "transient rods", visible in Fig. 1 and Fig. 2) located in 4 banks among the CABRI fuel rods are pressurized with ^{3}He gas.

The very fast depressurization of this strong neutron absorber into a discharge tank, through two flow channels (low and high flow rates), is finely adjusted to trigger the desired power pulse.

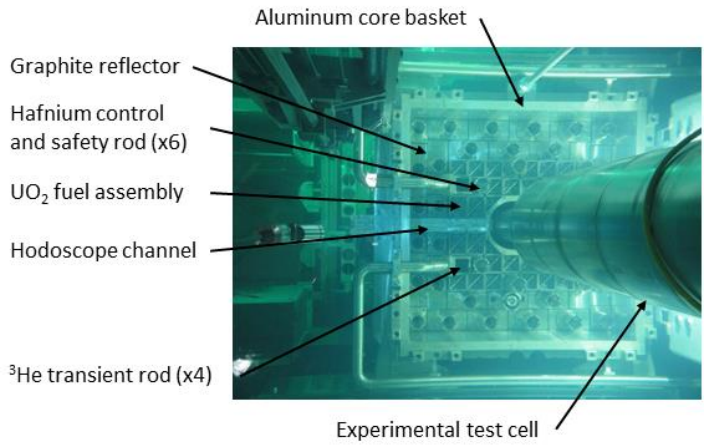

Fig. 1. View of the CABRI reactor from the top.

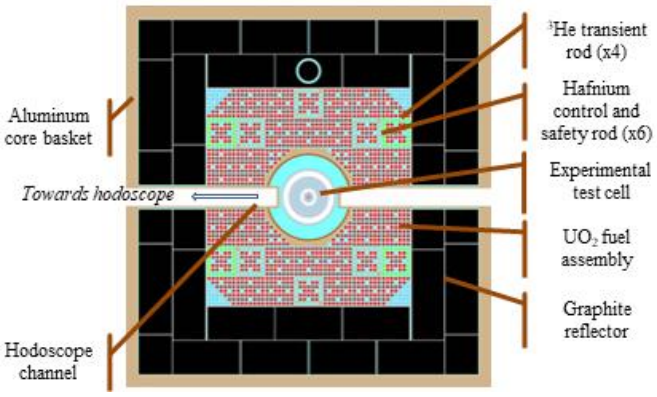

Fig. 2. Radial cross section of CABRI core

J. Di Salvo, S. Mirotta and V. Chevalier are with Nuclear Safety and Radiation Protection Institute I.R.S.N., 13108 St Paul Lez Durance, France (e-mail: Jacques.DiSalvo@irsn.fr).

The CABRI facility is equipped with two nondestructive measurement systems operated by IRSN:

- The IRIS facility, for performing X-ray radiography and tomography imaging before and after a power transient thanks to a linear electron accelerator, as well as quantitative gamma scanning analyses;
- The Hodoscope, an online fuel motion measurement system, which aims at analyzing the fuel motion deduced from the detection of fast neutrons emitted by the tested rod, in real time (with a time step of 1ms) during the transient [3].

This article presents a numerical model for the evaluation of:

- The Signal-to-Noise Ratio (SNR) of the hodoscope measurement system, which is a fundamental parameter to observe the fuel displacement (if any) during the power excursion.
- The scattering coefficient (α), which is required to determine the fuel ejected into the loop channel at pin failure [4].

In section II, a brief description of the meaning of the SNR will be given. In section III, the 2D model developed with MCNP6.2 [5] will be discussed. Furthermore, in section IV, results and a comparison to experimental values will be analyzed. Finally, conclusion and perspectives are given in section V.

II. Principles of Hodoscope Measurements

A. *Description of hodoscope equipment*

The hodoscope system, coupled with the CABRI reactor, is used to detect and measure online, during power transients, fuel displacement that may occur in the test rod. The system allows quantifying the amount of fuel ejected in the milliseconds following any potential failure, as well as the time-dependent axial fuel mass distributions, and monitoring the fuel clusters after failure [6].

The hodoscope system is made by a 3-m long, steel collimator, which is placed 1 m away from the test rod, and allows filtering in space and energy, neutrons coming from the core and from the test rod (Fig. 3). The collimator has 153 lines of sight arranged in a matrix of pixels of 51 rows and 3 columns, in order to assure both axial and radial discretization of the test rod, as well as the possibility to use the signal coming from one of these columns to normalize the signal during power excursion. For each line of sight of the collimator, two different detectors are installed, so that 306 detectors are managed by the hodoscope system. The first kind of sensors is ^{237}Np fission chambers (FC, energy threshold cross section at 600 keV) and the second kind is proton recoils counters (PR, energy threshold set by electronic system at 400 keV) [7].

These two different technologies of detectors are used in the CABRI reactor in order to follow all the experiments, from low power (~50 kW) up to 20 GW. PR sensors have a higher sensitivity and are therefore better suited for monitoring the low power part of the transient. Fission chambers follow the high power part of the transient. They proved to work well up to 21 GW, thanks to a specific dead time correction algorithm allowing to correct the linearity drift when the reactor power exceeds ~5 GW.

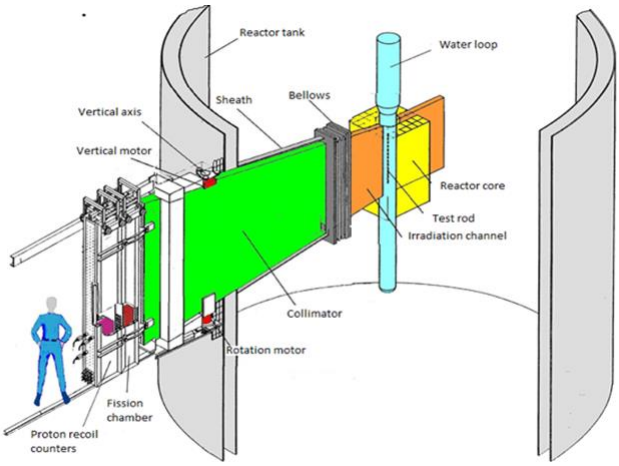

Fig. 3. General overview on the hodoscope equipment in the CABRI reactor.

The hodoscope collimator has three different degrees of freedom, for adjusting its position in front of the test rod, as presented in Fig. 4. The distance from the collimator aperture to the core axis may be adjusted manually in translation (x-axis), while two direct current motors are used to move the collimator vertically (the x-axis being the rotation axis) and rotate it (z-axis).

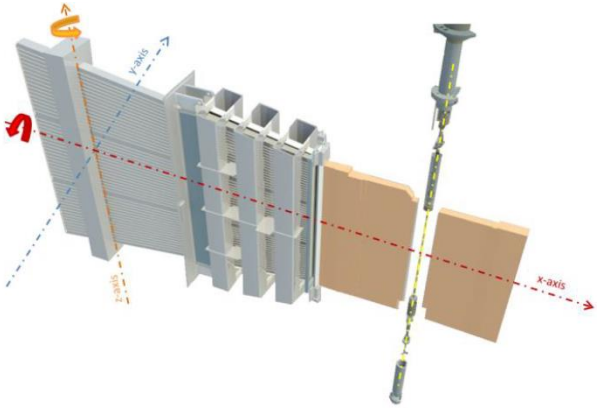

Fig. 4. Hodoscope collimator degrees of freedom in the CABRI reactor.

Before the measurements performed for a CABRI test, a collimator alignment campaign is required, to check that the collimator position is viewing the rod in the test cell [3]. This campaign follows an iterative way: during a power plateau of ~10 MW, the test rod will be scanned by the hodoscope while rotating the collimator. Once the data analyzed, a correction will be determined for the vertical motor position. A new power plateau will be performed to check this new position, so as to obtain the global alignment. At the end of this process, once the fissile length of the test rod has been determined (section II.C.1), the position of the collimator is assigned and will not change for the measurements during the transient, described in section II.C.2.

The geometry of three adjacent channels of one horizontal row is displayed in Fig. 5: it is possible to see that when the center column (channel 2) of the hodoscope collimator is placed in front of the test rod (diameter lower than 1 cm, and located at +4 m), detectors placed at the end of channel 2 aim at the test rod and therefore capture neutrons coming from it. It is not the

case for detectors placed at the end of the left and the right channels, which aims at the surrounding structure elements of the test loop (Fig. 2).

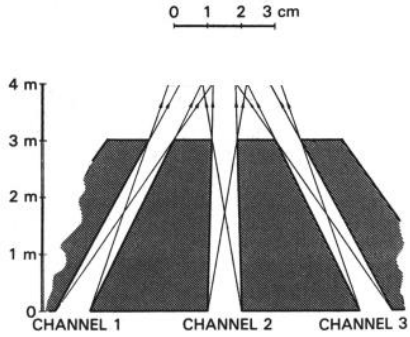

Fig. 5. Section of three horizontally adjacent collimator channels.

B. Signal-to-noise ratio definition

Only fast neutrons emitted by the test rod are useful for the measurements, all other neutrons (thermal neutrons, fast neutrons produced in CABRI driver fuel rods, etc.) do not contain any useful information for fuel displacement evaluation. Hence, the latter contribute to the "noise" of the measurement. Because of the detector's technology and collimator geometry, it is possible to measure only fast neutrons coming from the test rod (which contribute to the useful "signal").

The system of (1) for the detectors counting rate can be written when the collimator is placed in its centered position. The left column detector, as well as the right column detector, can measure fast neutrons coming from the reactor (n), with or without scattering, and those coming from the test rod, scattered into the structural materials of the test loop (αs). We define α as the scattering coefficient. Only the center column can measure the fast neutrons coming from the test rod (s), with or without scatter inside the test rod, in addition to the noise and the scattered neutrons.

$$\begin{cases} c_l = n + \alpha s \\ c_c = n + \alpha s + s \\ c_r = n + \alpha s \end{cases} \quad (1)$$

During the collimator alignment campaign, moving the collimator horizontally across the test section gives a maximum count rate if the corresponding pixel is aligned with the pin and a constant count rate if the test rod is completely beyond the pixel [3]. This justify that the amplitude of the scattered signal plus core background is the same for the three pixels of one collimator row [4].

Using the system (1), the ratio of the counting rates R can be written:

$$R = \frac{c_c}{\frac{c_l + c_r}{2}} = \frac{s}{n + \alpha s} + 1 = \frac{s}{N} + 1 \quad (2)$$

The signal-to-noise ratio "s/N" or SNR can be measured by the ratio between the counting rates of the hodoscope detectors. It is important to note that it is not possible to measure directly the signal over pure noise ratio "s/n", because the scattering coefficient has to be determined first.

The main difficulty in the measurement of the SNR is due to the small amount of neutrons coming from the test rod compared to all other neutrons present in the reactor.

C. Use of the SNR and the scattering coefficient for CABRI experiments

1) Measurement before the transient: example of fissile length determination

In this case, SNR is evaluated during a few MW power plateau, because many neutrons are required to gain statistics on the signals. During this measurement, the collimator moves horizontally (z-axis rotation) across the test section. Hence, each detector of the hodoscope system sees alternatively the test rod and the noise from the core. The software records the maximum of the count rate in front of each detector, and deduce the SNR by the ratio of the maximum count rate to the constant count rate obtained when the test rod is completely beyond the pixel.

Therefore, it is possible to obtain a SNR for each detector. Averaging its value across rows allows obtaining a mean SNR for each kind of detectors (Fig. 6). The fissile length is then deduced from this measurement: a pixel, for which SNR is greater than one, faces to fuel column.

We have to note that the poor energy discrimination of the PR counters results in a reduced SNR compared to the FC.

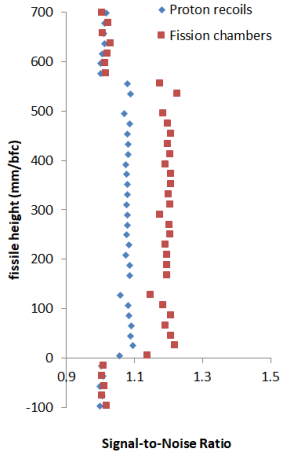

Fig. 6. Example of a typical SNR measurement for the two kind of detector technologies involved in the hodoscope equipment. *bfc : Bottom of Fuel Column.

It is interesting to note that the SNR indicator is quite independent of the Z-axis, hence independent of the control rods position: the results presented on Fig. 6 are obtained with the control rods inserted at the mid-plane of the core (around +300 mm/BFC).

2) Measurement during the transient

One of the most important measurement performed by the hodoscope is the evolution of the axial fuel distribution during the power transient for each hodoscope row. During this whole measurement, the collimator does not move: its position is assigned to the value deduced from the collimator alignment campaign. The SNR is directly deduced from the ratio between the counting rates of the hodoscope detectors, as expressed in (2). Thanks to its 1 ms time step acquisition, it is possible to see when and how the fuel is moving. This allows identifying phenomena at different axial locations and correlating them with signals from the test section instrumentation [8].

The hodoscope system plots the temporal evolution of the SNR as measured by the FC, compared to a reference SNR_0, evaluated during a 100 kW power plateau just before the transient. As an example, the $SNR(t)/SNR_0$ ratio, displayed in Fig. 7 for the hodoscope rows 19 to 25, describes fuel motions during a power transient. For a given row, a ratio greater than one (represented in green on the Fig. 7) means that the SNR at this time is higher than the SNR measured during the 100 kW power plateau. That corresponds to fuel accumulation in the water channel faced to the row, whereas a ratio lower than one, represented in red, can be interpreted as fuel removal.

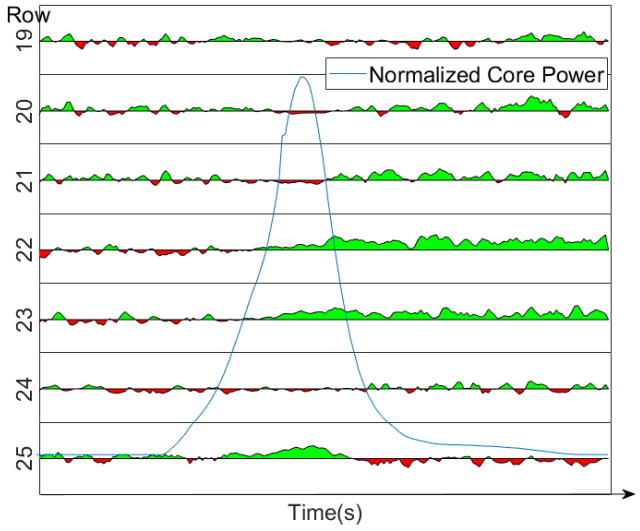

Fig. 7. Example of a typical SNR measurement during a transient: representation of fuel displacements

Transients that have only a limited impact on the test rod have already been tested, in the framework of the CIP program. During these experiments, the $SNR(t)/SNR_0$ ratio remains close to one, which means that the SNR indicator is quite insensitive to the depressurization of the transient rods.

The axial distribution of the fuel mass is also deduced from the hodoscope measurement. The distribution is estimated during different time periods (T_i) of interest to the experimentalist. The principle of this analysis, completely detailed in [4], requires two major steps:

- A double normalization of the signal, involving the use of the scattering coefficient. The aim is to correct the signal "s" with the pure noise "n", varying with power in the same way;
- A signal to mass conversion abacus, which is nowadays built thanks to the Monte Carlo MORET5 code [9], developed by IRSN. An idealized radial fuel distribution evolution during the transient is considered for each row and for each period of time T_i mentioned above, and applied to the $(s/n)_{Ti}/(s/n)_0$ ratio.

For the sodium loop configuration, the scattering coefficient was evaluated with a commissioning test [4], but, as it is not foreseen to measure it in the CABRI PWR loop, a specific methodology is proposed to evaluate this important parameter by means of a Monte-Carlo simulation.

III. Numerical Model

A. Geometry description

The CABRI reactor model was built using the MCNP6.2 Monte Carlo code, combined with the JEFF3.1.1 nuclear database [10]. A radial cross section of the model is displayed in Fig. 8. It is homogeneous along the Z-axis, 10-cm high, with reflective boundary conditions. The "kcode" option was used to perform MCNP6.2 runs. 3600 batches of 20 millions particles are simulated for each calculation.

This 2D simplification was needed, because of the poor statistic obtained with a 3D model, in the vicinity of the hodoscope detectors, which are located far from the reactor. As it will be detailed in the section III.B, this kind of simulations was intentionally chosen, in order to keep information on how and where the scoring particle was produced, so as to estimate the scattering coefficient.

Even if this model does not take into account the axial control rods position, and the related deformation of the axial flux, it has been shown that the SNR is quite independent of this parameter (Fig. 6): then a 2D model should be sufficient. In the same way, it has been considered that the helium pressure inside the transient rods plays a second order effect.

More precisely, the following simplifications were implemented in the 2D model:

- Axial grids were not modeled;
- Control and security rods were completely inserted into the reactor;
- The Helium 3 pressure into the transient rod was adjusted in order to keep the system almost critical: k_{eff} is around 0.99;
- The overall water pool, beyond the aluminum basket, was not taken into account, because of its distance to the core. However, the negligible effect of this assumption has been checked by comparing SNR calculations with and without the pool. Results were quite similar, but time calculation increase when the pool is present in the calculation, since much time is required to compute history of neutrons that are neither relevant for the SNR indicator nor for the scattering coefficient.

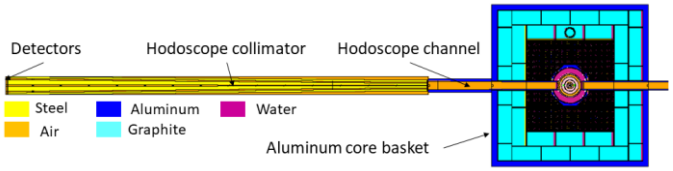

Fig. 8. MCNP6.2 radial cross section of CABRI reactor.

Once the CABRI model is implemented, different test rods were inserted in the center of the reactor, for different configurations of the central loop: the current PWR one and the previous sodium one.

B. Tally description

Tallies are used in MCNP6.2 to obtain an estimation of a physical observables into the model. For this study, volume averaged flux estimators (F4 tally) were considered. F4 tallies were separated into two energy bins, with a 600 keV boundary.

In this article fast fluxes correspond to all neutrons with an energy above 600 keV, which is the threshold value for ^{237}Np fission cross section. In the simulation, the neutrons above 600 keV coming from both the core and the test rod into the three detectors region are collected.

Scoring the fast fluxes for each detector is enough to estimate the SNR, but not sufficient to compute the scattering coefficient, since the knowledge of the birthplace of each neutron contributing to the tally results, as well as the part of the scattering effect, are required to obtain this parameter.

Hence, another option of the MCNP6.2 code was used to evaluate the proportion of neutrons produced into the test rod that scattered into the PWR loop structures. Tally tagging allows the user separating a tally into components based on how and where the scoring particle was produced. An option specifies how scatter is to be treated (i.e., whether the creation tag on a particle should be retained or a separate scatter tag be invoked). The choice is more specifically:

- Particles undergoing elastic scattering will lose their birthplace tag and they will be included into an "elastic scattered bin" (option TAG 1);
- Particles undergoing elastic scattering will retain their production tag. The "elastic scattered bin" will always be empty in this case (option TAG 3).

This feature requires a FU card which will detail the binning specifications for the tagged tally.

1) TAG 3 option calculation

In addition to the use of the TAG 3 option, two different bins were defined for the FU card:

1. Bin 1 takes into account source neutrons, born by fission, into the test rod;
2. Bin 2 takes into account (n,xn) neutrons and (n,n') inelastic scattered neutrons, produced into the test rod, by any neutrons (either coming from the driver fuel rods or the test rod).

For TAG 3 calculation, the sum of the contributions of bin 1 and bin 2 takes into account all neutrons produced into the test rod:

$$s + \alpha s = b_{1_{c,TAG3}} + b_{2_{c,TAG3}} \quad (3)$$

Hence, for each detector volume, it is possible to split the contribution to the tally which comes from the core (noise n) and the contribution to the tally due to the test rod (signal s + αs). As it is mentioned in the MCNP6.2 user's manual, if a particle has multiple production events, the tag will be for the last production event. Neutrons undergoing fission inside the test rod, followed by inelastic collisions in the PWR loop structures, would have the (n,n') tag and would not contribute to these two bins. This is a slight approximation to the part of the signal.

2) TAG 1 option calculation

Concerning the TAG 1 option, four different bins were defined for the FU card:

1. Bin 1 takes into account source neutrons, born by fission, into the test rod (the signal s, red line in Fig. 9). However, contrary to the previous case, neutrons undergoing elastic scattering after their production will lose their birthplace tag and will not contribute to this bin.
2. Bin 2 takes into account (n,xn) neutrons and (n,n') inelastic scattered neutrons produced into the test rod, by other neutrons (they are also part of the signal s, black dash-dotted line in Fig. 9);
3. Bin 3 takes into account all scattered neutrons independently from where they were born. This bin contains the scattered part of the signals αs (green dashed line in Fig. 9), a part of the signal s itself (black dashed line in Fig. 9), and all the neutrons coming from the driver fuel rods and being scattered at least once in their history (not represented in Fig. 9);
4. Bin 4 takes into account all the remaining neutrons. It consists of the special "everything else" bin, specified to collect any portion of tally that falls into no other bin. For instance, neutrons coming directly from the driver fuel rods, and not being elastically scattered, fall into this bin. One can also find neutrons coming originally from the test rod, and for which a (n,n') reaction occurs outside the test rod (green dash-dotted line in Fig. 9). As for TAG 3 option, this part cannot be recovered for the signal.

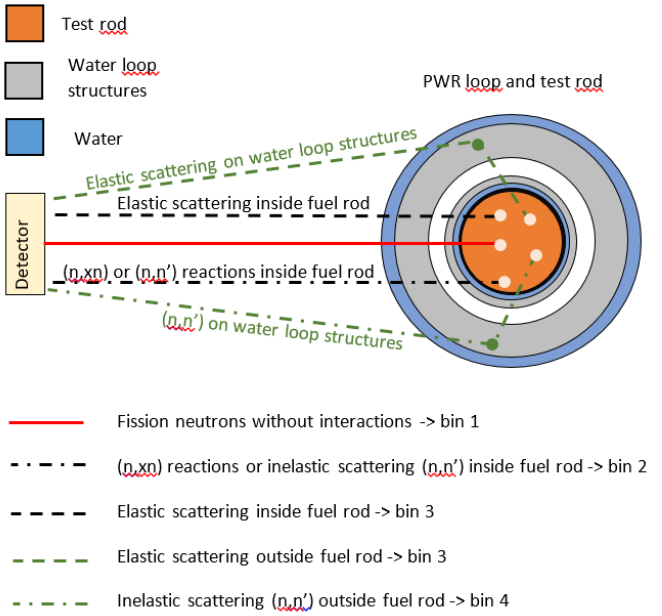

Fig. 9. All different neutron reactions produced by neutrons coming from the test rod (axial cut).

For TAG 1, a part of the signal, due to neutrons produced in the test rod, and elastically scattered inside the test rod, is put inside the bin 3. This contribution must be recovered for the complete evaluation of the signal, and is noted $\varphi_{el,c}$ in (4). The signal "s" can be computed by adding this term to the sum of the contribution of bin 1 and bin 2:

$$s = b_{1_{c,TAG1}} + b_{2_{c,TAG1}} + \varphi_{el,c} \quad (4)$$

The evaluation of this contribution is possible, using the neighboring channels, because they do not aim at the test rod and therefore do not include the signal s:

$$\varphi_{el,c} = b_{3_{c,TAG1}} - \frac{b_{3_{r,TAG1}} + b_{3_{l,TAG1}}}{2} \quad (5)$$

Hence, with TAG 1 option, it is possible to obtain the pure signal "s", separately from the contribution due to neutrons coming from the test rod and elastically scattered into the PWR loop structures (αs).

3) Combination of the two calculations

Finally, it is possible to obtain the scattering coefficient for the CABRI reactor by combining the results coming from the two calculations:

$$\alpha = \frac{s+\alpha s}{s} - 1 = \frac{b1_{c,TAG3} + b2_{c,TAG3}}{b1_{c,TAG1} + b2_{c,TAG1} + \varphi_{el,c}} - 1 \quad (6)$$

IV. Results

Results are presented in this section with uncertainties evaluated at 2σ, which means a confidence interval of 95%. This section will detail, for the current PWR loop implemented in the CABRI reactor, as well as for the previous sodium loop:

- the results of the evaluation of the SNR for different test rods;
- the evaluation of the scattering coefficient.

A. SNR results

1) PWR loop

Thanks to the methodology presented in the previous sections, it is possible to evaluate the SNR ratio as well as the scattering coefficient. Table I shows the results obtained for an aluminum test rod (ALU, case study for a non-fissile material), fresh UO_2 test rod (F_UO_2, PWR rod geometry, 4.2% ^{235}U enrichment), a depleted MOX test rod (I_MOX, burn-up approximatively equal to 45 GWd/t).

Uncertainties on the tallied values c_l, c_r and c_c are relative uncertainties given at 2σ. The uncertainties on SNR ratio are absolute uncertainties (2σ). In this theoretical case, the value of the SNR is close to 0 as expected, because no neutron coming from fission can be created from the test rod.

For the F_UO_2 fuel rod, no radionuclide inventory due to previous irradiation has to be computed, so that the discrepancy between the simulation and the experiment performed with this fuel rod can only be attributed to the model (approximations due to the 2D hypothesis, operating conditions, geometrical errors as well as bias due to nuclear data). The measured value obtained during the reactor power plateau was 27.0% ± 2.0%. Comparison of calculated and experimental results are quite in good agreement.

For the I_MOX fuel rod, the discrepancy observed between the simulation and the experiment is more important, reaching 8%. The slight overestimation already observed for the F_UO2 fuel rod, is increased in the case of the I_MOX, for which effects of the technological uncertainties of the model could be more significant. A part of this discrepancy could also be due to the inventory calculation method used to assess the initial composition of the fuel rod in the calculation.

Hence it is interesting to make the same evaluation for the sodium loop conditions for which a more extended experimental database is available.

TABLE I
SNR AND C/E COMPARISON, FOR TEST ROD LOADED INTO THE PWR LOOP

Neutron flux (a.u)	ALU test rod	F_UO2 test rod	I_MOX test rod
c_l: left channel	3.71 10^{-08} (1.4%)	4.22 10^{-08} (1.4%) [a]	4.07 10^{-08} (1.4%)
c_c: center channel	3.81 10^{-08} (1.4%)	5.41 10^{-08} (1.2%)	5.23 10^{-08} (1.2%)
c_r: right channel	3.75 10^{-08} (1.4%)	4.12 10^{-08} (1.4%) [a]	4.09 10^{-08} (1.4%)
SNR: calculation	2.2% ± 1.8%	29.5% ± 1.8%	28.1% ± 1.8%
SNR: experiment	-	27.0% ± 2.0%	20.0% ± 2.0%

[a] Even if, for the fluxes in the left and right channels, there is only a limited recovery of their error bars, their values have been checked with a second calculation (based on a new random seed). The values obtained, 4.19 10^{-08} (1.4%) for the left channel and 4.15 10^{-08} (1.4%) for the right channel, were consistent with the first calculation, and led to the same average value for the neighboring channels.

2) Sodium loop

Table II shows the results obtained for:

- a fresh UO_2 test pin, fast reactor reference pin of 20.0% ^{235}U enrichment, 6.4-mm pellet diameter, but of only half the fissile height of the driver fuel rods (F_UO2);
- an irradiated UO_2 PWR test rod geometry (I_UO2, burn-up approximatively equal to 70 GWd/t);
- an irradiated MOX PWR test rod geometry (I_MOX, burn-up approximatively equal to 45 GWd/t).

Experimental results for F_UO2 test rod, presented in [4], were obtained with a special calibration experiment: the central row of the collimator was aligned with the F_UO2 test pin. This experiment was dedicated to investigate the composition of the total count rates and therefore to measure the scattering coefficient. The SNR ratio was estimated as a byproduct. However, no experimental uncertainties were given and they have been reconstructed for this study by using the experimental dispersion on normalized count rates, leading to a rather high value of ten percent (2σ), compared to values obtained for the other experiments.

TABLE II
SNR AND C/E COMPARISON, FOR TEST ROD LOADED INTO THE SODIUM LOOP

Neutron flux (a.u)	F_UO2 test rod	I_UO2 test rod	I_MOX test rod
c_l: left channel	5.09 10^{-08} (1.2%)	4.64 10^{-08} (1.4%)	4.82 10^{-08} (1.2%)
c_c: center channel	7.92 10^{-08} (1.0%)	5.65 10^{-08} (1.2%)	6.52 10^{-08} (1.0%)
c_r: right channel	5.06 10^{-08} (1.2%)	4.68 10^{-08} (1.4%)	4.84 10^{-08} (1.2%)
SNR: calculation	56.2 % ± 1.8%	21.3 % ± 1.7%	34.9 % ± 1.7%
SNR: experiment	50.4 % ± 10.0%	15.6 % ± 2.0%	27.5 % ± 2.0%

To conclude, it could be noticed that for all the simulations in the sodium loop configuration, a discrepancy of about 5 to 7 percentage points with the experimental values has been obtained. These results were considered as acceptable, because the goal of this study was first to be able to get a tool dedicated to achieve reasonable predictions of the future SNR ratios met in the CABRI programs. The second objective was to use this tool for the scattering coefficient evaluation.

B. Scattering coefficient evaluation

Calculations with different tally tagging as detailed in the section III.B have been performed to estimate the scattering coefficient, for PWR and sodium loop configurations.

The 95% confidence interval for the scattering coefficient is respectively [20.7%; 23.3%] and [19.2%; 20.8%] for the PWR loop and sodium loop configurations (Table III). These values

are coherent with the one found experimentally for the sodium loop configuration, which was measured to be 22.8% (according to [4], without uncertainties associated to this value). More scattering effect could be expected in the PWR loop than in the sodium loop configuration.

Uncertainties presented here are only due to the convergence of the Monte Carlo calculations. They represent only a limited part of the total uncertainty as presented in the section IV.C, especially for the scattering coefficient.

TABLE III
TALLY SCORE PERFORMED FOR SCATTERING COEFFICIENT EVALUATION

Tally option	Symbol	Flux (a.u) PWR loop	Flux (a.u) Sodium loop
TAG3	$b_{1_{c,TAG3}}$	1.54 10^{-08} (2.2%)	3.23 10^{-08} (1.6%)
	$b_{2_{c,TAG3}}$	3.97 10^{-10} (12.6%)	5.66 10^{-10} (10.6%)
TAG1	$b_{1_{c,TAG1}}$	9.89 10^{-09} (2.6%)	2.20 10^{-08} (1.8%)
	$b_{2_{c,TAG1}}$	2.07 10^{-10} (17.4%)	3.35 10^{-10} (14.0%)
	$b_{3_{l,TAG1}}$	3.98 10^{-08} (1.4%)	4.77 10^{-08} (1.2%)
	$b_{3_{c,TAG1}}$	4.24 10^{-08} (1.4%)	5.26 10^{-08} (1.2%)
	$b_{3_{r,TAG1}}$	3.93 10^{-08} (1.4%)	4.78 10^{-08} (1.2%)
	α	22.0% ± 1.3%	20.0% ± 0.8%

C. Uncertainty estimation (PWR loop conditions)

1) Sensitivity to technological uncertainties

As mentioned before, some assumptions are made in the 2D model, which does not take into account the axial control rod position, as well as the exact ^{3}He pressure in the transient rods. These assumptions have a negligible effect on the SNR and scattering coefficient values, as explained in the section II.

Some biases of the model can also be due to slight approximations on thermal-hydraulic conditions of the different experiments.

In this work, we focused the sensitivity study on two main geometrical parameters:

(1) The amount of water between the hodoscope channel and the safety tube containing the test rod which arises from the clearance gap between these mechanical pieces (Fig. 10).
This value is not exactly known, considering the space available for the positioning of the different pieces, an uncertainty of ±3 mm (2σ) is realistic. The clearance gap has a significant impact on the scattering coefficient as it contains the major part of water between the hodoscope detectors and the test rod. The other water gaps, inside the device, are thinner and their thickness are quite well known. The sensitivity to this parameter was deduced from two calculations, the first one considering a 7-mm clearance gap and the second one by joining the hodoscope channel to the safety tube so as to remove the space between them.

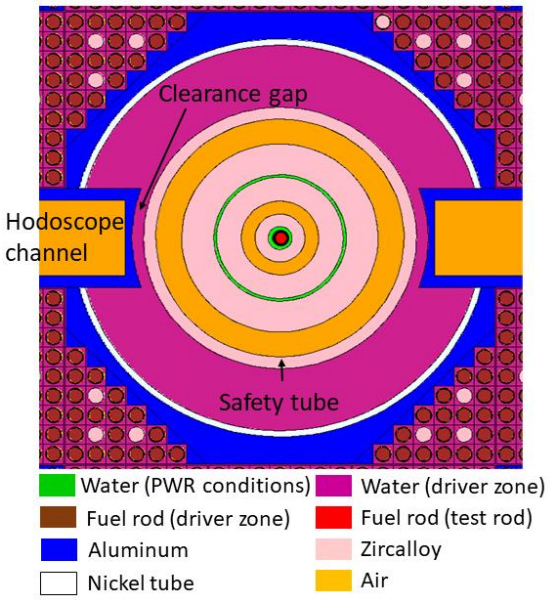

Fig. 10. Zoom on PWR loop and its interface with the hodoscope channel (Radial cut).

(2) The distance between the collimator aperture and the axial axis of the core. A metrology campaign has been performed at the renovation of the PWR loop and a value of 1020±10 mm (2σ) was measured for this parameter. As the aperture collimator is far from the PWR loop, this parameter is supposed to have only a small impact on the scattering coefficient. On the contrary, it could have an impact on the SNR because of the geometrical effects on the shadow areas of each line of sight (Fig. 5). The sensitivity to this parameter was obtained by moving the collimator 2 cm away from its reference position while leaving the hodoscope channel in the same location (i.e. not changing the clearance gap).

In the following all uncertainties are given at 2σ. For the SNR ratio, the sensitivity calculated (Table IV) associated to the technological uncertainties mentioned above leads to complete the statistical uncertainty (about 1.8%) with a technological uncertainty of the same order of magnitude: 2.1%. For the scattering coefficient, as expected, only the clearance gap influences the uncertainty, and the impact of the technological uncertainty (5.4%) predominates the statistical uncertainty (1.3%). The scattering coefficient is very sensitive to the geometrical configuration of the PWR loop.

TABLE IV
SENSITIVITY TO TECHNOLOGICAL PARAMETERS FOR F_UO2 TEST ROD LOADED INTO THE PWR LOOP

Quantity	SENSITIVITY COEFFICIENT	
	(1) clearance gap between hodoscope and safety guide	(2) distance hodoscope collimator / center of core
s/N	0.5% / mm	1.4% / cm
α	1.8% / mm	-

2) Sensitivity to nuclear database

These calculations are performed to get an estimation of the effect of the choice of a particular nuclear database. As shown in Table V, the impact of the nuclear database on the SNR ratio is limited. For the α coefficient, a discrepancy can be observed between JEFF3.1.1 [10] and ENDF/B-VII.0 [11] evaluations. An expanded uncertainty of 3% covering this discrepancy will be added to the technological and statistical uncertainties.

TABLE V
NUCLEAR DATA BASE EFFECT ON THE SNR RATIO AND THE SCATTERING COEFFICIENT – PWR LOOP CONDITIONS

Quantity	NUCLEAR DATA BASE	
	JEFF3.1.1	ENDF/B-VII.0
s/N (F_UO_2)	29.5% ± 1.8%	29.7% ± 1.8%
s/N (I_MOX)	28.1% ± 1.8%	27.7% ± 1.8%
s/N (ALU)	2.2% ± 1.8%	0.9% ± 1.8%
α	22.0% ± 1.3%	24.6% ± 1.5%

3) Estimated uncertainties on the SNR and scattering coefficient

The major part of the uncertainties may be included in the previous estimations, and the whole uncertainty is computed as the quadratic sum of each contribution, then rounded up.

For the SNR, a final 2σ uncertainty of 3% is obtained with the following contributions:

- Statistical uncertainty: 1.8%;
- Technological uncertainty: 2.0% coming from the clearance gap uncertainty (1.5%) and the hodoscope collimator distance to the test rod (1.4%).

For the scattering coefficient, the repartition is considered as follows, leading to a final uncertainty of 6.5%:

- Statistical uncertainty: 1.3%;
- Technological uncertainty: 5.4%;
- Nuclear data uncertainty: 3.0%.

V. CONCLUSION

This work presents results obtained with a newly implemented, simplified, 2D model of the CABRI reactor. The purpose was to determine the Signal-to-Noise Ratio (SNR) as well as the scattering coefficient (α), both involved in the post-processing of the hodoscope measurements.

This work showed that the SNR measured for a representative set of fuel samples (fresh UO_2 and 45 GWd/t irradiated MOX pins) in the PWR loop of CABRI was determined with a +6% accuracy and an uncertainty of 3% at 2σ. The new model can also play a tremendous role to predict the impact of any modification of the test loop on the hodoscope measurements, particularly in the phase of conception of new experimental programs. For the PWR loop configuration, the calculated scattering coefficient found in this work (22.0%±6.5%) will be introduced in the quantitative analysis of the hodoscope measurements.

Regarding future work, additional data on fresh fuel pins measured in the sodium loop configuration were recently found and could extend the validation of the SNR calculations. Another possible work would be to extend the sensitivity studies to include more recent nuclear data libraries and more test fuel samples (e.g. irradiated MOX and UOX).

APPENDIX: NOMENCLATURE

s	Signal of neutrons coming from the test rod
α	The scattering coefficient
n	Noise, neutrons coming for the CABRI reactor
N	$n + \alpha s$
c_i	Counting rate of the ith column (r=right, c=center, and l=left)
$b_{j_{i,TAG1}}$	The value into bin jth, of the ith column (r=right, c=center, and l=left) evaluated with TAG 1 option: - 1 = test rod signal, direct contribution - 2 = (n,xn) and (n,n') contribution of neutrons coming from test rod - 3 = all elastic scattered neutrons - 4 = "everything else" tag, all other neutrons

REFERENCES

[1] "Reactivity Initiated Accident transient testing on irradiated fuel rods in PWR conditions: The CABRI International Program". Biard B. et al. Annals of Nuclear Energy, Vol **141**, 15 June 2020, 107253. https://doi.org/10.1016/j.anucene.2019.107253

[2] "Renovation, improvement and experimental validation of the Helium-3 transient rods system for the reactivity injection in the CABRI reactor". Duc B. et al. Proc of IGORR 2014 conference, Bariloche, Argentina, November 2014

[3] "The CABRI fast neutron Hodoscope: Renovation, qualification program and first results following the experimental reactor restart". Chevalier V., Mirotta S., Guillot J., Biard B. EPJ Web of Conferences, Volume **170**, 10 January 2018

[4] "Quantitative fuel motion determination with the CABRI fast neutron hodoscope: Evaluation methods and results". Baumung K., Augier G. Nuclear Technology, vol **96**, p. 302-311, June 1991

[5] "MCNP® user's manual. Code version 6.2. Manual Rev. 0" Werner C. J. editor. LA-UR-17-29981. October 27, 2017

[6] "The CABRI fast neutron hodoscope". Baumung K., Böhnel K., Bluhm H. Nuclear Technology, vol **71**, p. 353-365, Oct. 1985

[7] "The CABRI fast neutron Hodoscope: calibration campaign results". Chevalier V., Mirotta S., Monchalin N., Guillot J. The European Research Reactor Conference, the annual gathering of the research reactor community in Europe, RRFM, Oct 2020, HELSINKI (on line), Finland. (https://hal.archives-ouvertes.fr/hal-03080772).

[8] "CABRI test events monitoring through three measurement systems". Grando Q., Lebreton L., Chevalier V., Di Salvo J., Eymery S., Gaillard C., Monchalin N., Guillot J. EPJ Web of Conferences, Volume **253**, 19 November 2021

[9] "Capabilities overview of the MORET 5 Monte Carlo code". Cochet, B. et al. Joint International Conference on Supercomputing in Nuclear Applications and Monte Carlo 2013 (SNA + MC 2013), La cité des Sciences et de l'Industrie, Paris, France, October 27-31, 2013

[10] "The JEFF-3.1.1 Nuclear Data Library. Validation results from JEF2-2 to JEFF-3.1.1". JEFF Report 22, A. Santamarina et al., ISBN 978-92-64-99074-6. © OECD 2009.

[11] "ENDF/B-VII.0: Next Generation Evaluated Nuclear Data Library for Nuclear Science and Technology" M.B. Chadwick et al. Nuclear Data Sheets Vol 107, Issue 12, December 2006, Pages 2931-3060. (https://doi.org/10.1016/j.nds.2006.11.001).